NUCL SCI TECH (2019) 30:58
https://doi.org/10.1007/s41365-019-0579-1

Study on element detection and its correction in iron ore concentrate based on a prompt gamma-neutron activation analysis system

Long Zhao[1,2] · Xu Xu[1] · Jing-Bin Lu[1] · Ya-Lin Gong[2] · Xiang-Lin Li[3] · Wei Zhang[2] · Qing-Min Shang[2] · Qing-Feng Song[2] · Yan-Feng Li[2]

Received: 19 May 2018 / Revised: 13 September 2018 / Accepted: 20 October 2018 / Published online: 13 March 2019

Abstract A prompt gamma-neutron activation analysis (PGNAA) system was developed to detect the iron content of iron ore concentrate. Because of the self-absorption effect of gamma-rays and neutrons, and the interference of chlorine in the neutron field, the linear relationship between the iron analytical coefficient and total iron content was poor, increasing the error in the quantitative analysis. To solve this problem, gamma-ray self-absorption compensation and a neutron field correction algorithm were proposed, and the experimental results have been corrected using this algorithm. The results show that the linear relationship between the iron analytical coefficient and total iron content was considerably improved after the correction. The linear correlation coefficients reached 0.99 or more.

Keywords Prompt gamma-neutron activation analysis · Self-absorption · Energy spectrum · Compensation · Correction · Iron ore concentrate

This work was supported by the National Key Scientific Instrument and Equipment Development Projects (No. 2012YQ240121), Liaoning science and technology project (No. 2017220010), and Changchun Science and Technology Bureau Local Company and College (University, Institution) Cooperation Projects (No. 17DY023).

✉ Jing-Bin Lu
ljb@jlu.edu.cn

[1] College of Physics, Jilin University, Changchun 130012, China

[2] Dandong Dongfang Measurement & Control Technology Co., Ltd, Dandong 118002, China

[3] Hunan First Normal University, Changsha 410205, China

1 Introduction

Prompt gamma-neutron activation analysis (PGNAA) is a form of rapid and non-contact multi-elemental analysis technique, which has been widely used for element detection and analysis in various fields, such as cement, coal, and mineral resource industries [1–15]. With real-time, online detection results from PGNAA, a factory can adjust the control parameters simultaneously and hence improve the product quality. The PGNAA technique is based on the detection of prompt gamma-rays emitted through thermal neutron capture (n_{th}, γ) or neutron inelastic scattering (n, n' γ) [1, 2]. It can distinguish the elemental categories in the material from the characteristic γ-ray energy spectrum and estimate the element content from the intensities of characteristic energy peaks in the spectrum [3, 4]. PGNAA technology involves neutron moderation technology, characteristic gamma-ray energy spectrum technology, and the spectrum deconvolution technique [5–10]. At present, PGNAA technology is widely used to detect high contents of light elements or low contents of heavy elements in a sample, such as calcium, silicon, iron, and aluminum in cement [1, 4, 12]. Owing to the self-shielding effect of gamma-rays and neutrons in some heavy elements [16–20], which increases the error of PGNAA technology in the detection of heavy element concentrates, the applications of PGNAA technology using heavy elements are limited.

In the steel industry, the sintering process is quite sensitive to the iron ore concentrate grade; thus, real-time and accurate detection of the grade is very important to improve the sintering process and sinter quality. Here, a new correction algorithm, with gamma-ray self-absorption and neutron self-absorption considered, for the detection of

iron ore concentrate grade by PGNAA is developed. By means of the new correction algorithm, the linear correlation between the iron analytical coefficient and the total iron content has been improved from 0.79747 to 0.99886, and the influence of chlorine in the sample on the detection error has been reduced as well. As a result, an effective and accurate real-time detection of the iron ore concentrate grade during the sintering process has been demonstrated based on PGNAA technique and the new correction algorithm.

2 Experiment

2.1 Equipment setup

A PGNAA was used to detect the iron content in iron ore concentrate in the experiment. Figure 1 schematically shows the equipment setup [15]. Two 20 μg ^{252}Cf neutron sources were placed in the source chamber. Two 5 inch × 5 inch (diameter × height) NaI detectors were used as the prompt gamma-ray detector. The experimental equipment was produced by DFMC, which was suitable for a one-meter-wide belt. The spectrum acquisition time of each sample was set to 3600 s. Because of the strong shielding ability of iron on gamma-rays, the characteristic gamma-ray of a sample containing iron should have strong gamma-ray self-absorption [21]. To measure the self-attenuation degree of gamma-rays, one gamma-ray attenuation degree detection system was installed after the PGNAA, which included a ^{137}Cs gamma-radiation source installed below the belt and a γ-ray detector installed above the belt, as shown in Fig. 2.

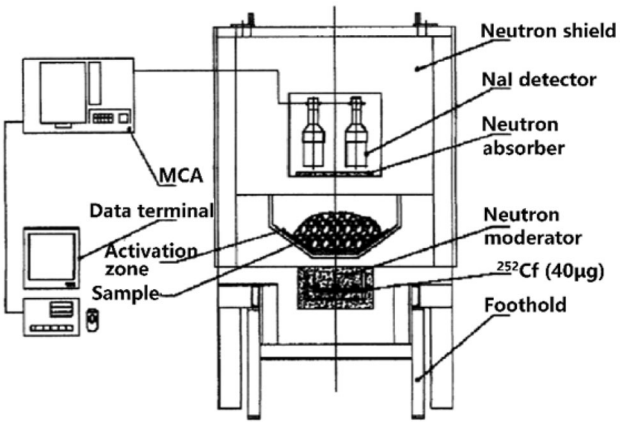

Fig. 1 PGNAA device structure

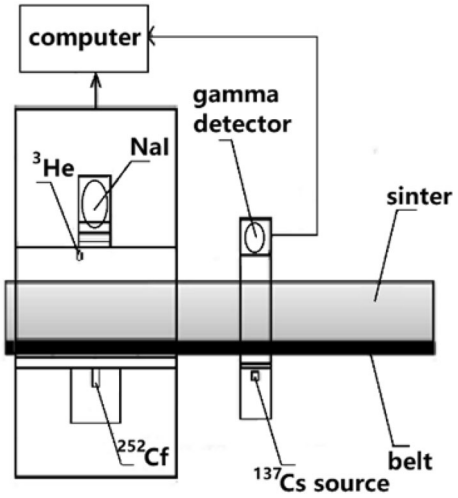

Fig. 2 System structure diagram

2.2 Sample preparation and experimental load

Six calibration samples and nine validation samples, with differing iron contents, were prepared for the experiment. Silicon, magnesium, calcium, and chlorine interference elements were added in sample 2-1# ∼ 2-9# to simulate a real test. The compositions of the calibration samples are shown in Table 1, and the compositions of the verification samples are listed in Table 2.

An inflection curve is observed for the analytical coefficient between the deconvolution coefficient of iron and the sample load owing to the gamma-ray self-attenuation effect, as shown in Fig. 3. In Fig. 3, the linear region is between 60 and 130 kg. To obtain more rational results, 110 kg was selected as the experimental load in this study.

2.3 Gamma-ray self-absorption correction

The following compensation formula [22] for gamma-ray self-absorption is used to correct for self-attenuation:

$$I_{0_{E_i}} = I_{E_i} \exp\left(\frac{-\mu_{mE_i}}{\mu_0} \ln\left(\frac{N}{N_0}\right)\right) (1\ \text{MeV} \le E_i \le 10\ \text{MeV}), \quad (1)$$

where $I_{0_{E_i}}$ is the energy spectrum without attenuation, I_{E_i} is energy spectrum obtained by the PGNAA detector, μ_{mE_i} is the characteristic gamma-ray mass attenuation coefficient with energy E_i, μ_{mE_i} is related to the atomic number of the material and the energy of the gamma-ray, N is the detector count rate of the gamma-ray attenuation degree detection system when there is material on the belt, N_0 is the detector count rate of the gamma-ray attenuation degree detection system with no material on the belt, and μ_0 is the mass attenuation coefficient of the ^{137}Cs radioactive source with energy equal to 0.662 MeV.

Table 1 Chemical composition of calibration samples, wt% relative to dry material

Sample	TFe	SiO_2	CaO	MgO	Cl	Other
1-1#	46.34 ± 0.16	9.19 ± 0.08	9.8 ± 0.07	4.98 ± 0.1	1.22 ± 0.09	8.61
1-2#	48.23 ± 0.16	9.88 ± 0.08	9.92 ± 0.07	1.95 ± 0.08	0.94 ± 0.07	8.41
1-3#	50.75 ± 0.16	8.34 ± 0.08	8.14 ± 0.06	2.62 ± 0.08	0.51 ± 0.04	7.89
1-4#	54.6 ± 0.16	6.45 ± 0.08	6.73 ± 0.06	1.45 ± 0.08	0.27 ± 0.02	7.1
1-5#	52.85 ± 0.16	6.89 ± 0.08	5.54 ± 0.06	3.36 ± 0.08	0.69 ± 0.05	8.02
1-6#	58.1 ± 0.16	4.14 ± 0.06	4.53 ± 0.06	0.51 ± 0.07	0.33 ± 0.03	7.49

TFe total ferrous content

Table 2 Chemical composition of check samples, wt% relative to dry material

Sample	TFe	SiO_2	CaO	MgO	Cl	Other
2-1#	47.29 ± 0.16	9.54 ± 0.08	9.86 ± 0.07	3.47 ± 0.08	1.08 ± 0.08	8.49
2-2#	49.49 ± 0.16	9.11 ± 0.08	9.03 ± 0.07	2.29 ± 0.08	0.73 ± 0.05	8.14
2-3#	50.54 ± 0.16	8.39 ± 0.08	7.73 ± 0.06	2.66 ± 0.08	0.82 ± 0.06	8.2
2-4#	52.68 ± 0.16	7.4 ± 0.08	7.44 ± 0.06	2.04 ± 0.08	0.39 ± 0.03	7.47
2-5#	48.55 ± 0.16	8.77 ± 0.08	8.97 ± 0.07	3.8 ± 0.1	0.87 ± 0.06	8.23
2-6#	51.8 ± 0.16	7.62 ± 0.08	6.84 ± 0.06	2.99 ± 0.08	0.6 ± 0.04	7.95
2-7#	55.48 ± 0.16	5.52 ± 0.06	5.04 ± 0.06	1.94 ± 0.08	0.51 ± 0.04	7.73
2-8#	53.73 ± 0.16	6.67 ± 0.08	6.14 ± 0.06	2.41 ± 0.08	0.48 ± 0.04	7.54
2-9#	56.35 ± 0.16	5.3 ± 0.06	5.63 ± 0.06	0.98 ± 0.07	0.3 ± 0.02	7.29

TFe total ferrous content

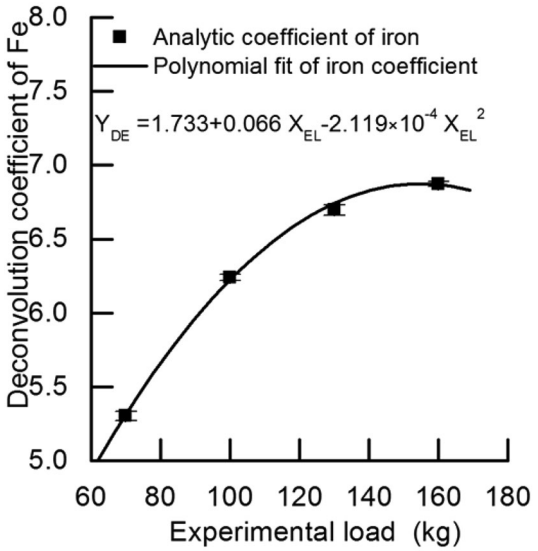

Fig. 3 Analytic coefficients of iron with different loads

The linear absorption coefficient, μ, of the material is defined as follows:

$$\mu = \sum N_i \sigma_i^{\gamma} \quad i = \text{Ca, Si, O, Mg, Cl, Fe,} \tag{2}$$

where N_i is the atomic density of each element and σ_i^{γ} stands for the total microscopic photon atomic cross section.The calculation formula of parameter N_{element} is defined as follows:

$$N_{\text{element}} = \frac{m_\rho}{\sum M_i f_i} f_{\text{element}} \times N_{\text{A}} \times 10^{-24} \quad i = \text{Ca, Si, O, Mg, Cl, Fe,} \tag{3}$$

where m_ρ is the mass density of the material being measured, M_i is the atomic weight of each element, f_i is the proportion of each element, f_{element} is the proportion of current element, and N_{A} is Avogadro's constant.

The characteristic gamma-rays are not all produced at the bottom of the detection area. They are generated at every location in the detection area; thus, the final correction formula, with a correction factor k, can be rewritten as follows:

$$I_{0E_i} = I_{E_i} \exp\left(\frac{-\mu_{mE_i}}{\mu_0} k \ln\left(\frac{N}{N_0}\right)\right) \ (1 \text{ MeV} \le E_i \le 10 \text{ MeV}). \tag{4}$$

The main materials in the iron ore concentrate are calcium oxide, silicon dioxide, ferrous oxide, ferric oxide, magnesium oxide, and chlorine. The corresponding composition of each material is listed in Table 3. Iron ore contains six elements: oxygen, magnesium, silicon, calcium, iron, and chlorine; the atomic proportions (f_i) of each element are listed in Table 4. The linear absorption coefficient, μ, of iron ore concentrate can be calculated from Eqs. 2 and 4, and the atomic proportions are listed in Table 4. The $\frac{-\mu_{mE}}{\mu_0}$ data for each element are listed in Table 5.

Using the characteristic energy spectrum, I_{E_i} (1 MeV $\leq E_i \leq$ 10 MeV), constant $\frac{-\mu_{mE_i}}{\mu_0}$ (1 MeV $\leq E_i \leq$ 10 MeV), and count rate N and N_0 in Eq. 4, the energy spectrum after compensation, $I_{0_{E_i}}$ (1 MeV $\leq E_i \leq$ 10 MeV), is obtained.

The gamma-ray self-absorption compensation parameters and data of the six calibration samples are listed in Table 6. The energy spectra before and after gamma-ray self-absorption compensation are shown in Fig. 4a, b, respectively. The relationship between the analytical coefficient and iron content, before and after gamma-ray self-absorption compensation, is shown in Fig. 5a, b, respectively.

2.4 Neutron self-absorption correction

Self-absorption in the PGNAA technique is comprised of two parts: gamma-ray self-absorption and neutron self-absorption [16–18]. A bigger neutron-absorption cross section will result in more neutron self-absorption. The neutron capture reaction cross section and characteristic gamma-ray energy of different materials are listed in Table 7 [19].

Previous work regarding neutron self-absorption correction [20] by Professor Wen-bao Jia is compared with the current iron ore concentrate detection experiment listed in Table 8. It is clear that the total neutron capture cross section of iron is quite strong in the iron ore concentrate detection experiment, contrasting with the experiment by Professor Jia, which means the influence of sample thickness on detection results is higher than that of previous evaluation.

The experimental samples contain silicon, calcium, magnesium, chlorine, and other interfering elements. The test results of iron can be disturbed by these elements. The iron element test result, found by a PGNAA, can be expressed by the following formula:

$$m'_{\mathrm{Fe}} = K\frac{N_{\mathrm{Fe}}\sigma^{\mathrm{n}}_{\mathrm{Fe}}}{\sum N_i\sigma^{\mathrm{n}}_i} \quad i = \mathrm{Ca, Si, O, Mg, Cl, Fe,} \tag{5}$$

where m'_{Fe} is the iron grade, as detected by the PGNAA, and K is a constant representing all other contributing factors. σ^n_i is the neutron-absorption cross section of each element listed in Table 7.

The formula for the contribution of each element (excluding iron) to the measurement error of iron is as follows:

Table 3 Chemical composition of iron ore, wt% relative to dry material

Material	CaO	SiO_2	TFe	FeO	MgO	Cl
Mass ratio	10.58	5.14	56.33	7.28	2.51	0.25

TFe total ferrous content

Table 4 Atomic proportion of the element of iron ore (f_i)

Element	Ca	Si	Mg	Fe	O	Cl
Proportion	0.059933	0.0271758	0.019906	0.3099326	0.5830522	0.002232

Table 5 $\frac{-\mu_{mE}}{\mu_0}$ data for each element

Element	Cl	Hg	Ca	Si		Mg	Fe		O
Energy (MeV)	6.11	5.967	6.42	3.539	4.934	3.916	7.631	7.646	3.272
$\frac{-\mu_{mE}}{\mu_0}$	− 0.393	− 0.395	− 0.388	− 0.464	− 0.415	− 0.447	− 0.377	− 0.377	− 0.478

Table 6 Gamma-ray self-absorption compensation parameters and data of six calibration samples

Sample	1-1#	1-2#	1-3#	1-4#	1-5#	1-6#
TFe (wt%)	46.34 ± 0.16	48.23 ± 0.16	50.75 ± 0.16	54.60 ± 0.16	52.85 ± 0.16	58.10 ± 0.16
A_{Fe}	6.616	6.799	7.445	7.273	7.996	7.841
N/N_0	0.582	0.501	0.528	0.479	0.608	0.452
A^1_{Fe}	7.648	8.428	9.063	9.36	9.008	10.594

A_{Fe} means analytic efficient of iron before gamma-ray self-attenuation correction

A^1_{Fe} means analytic efficient of iron after gamma-ray self-attenuation correction

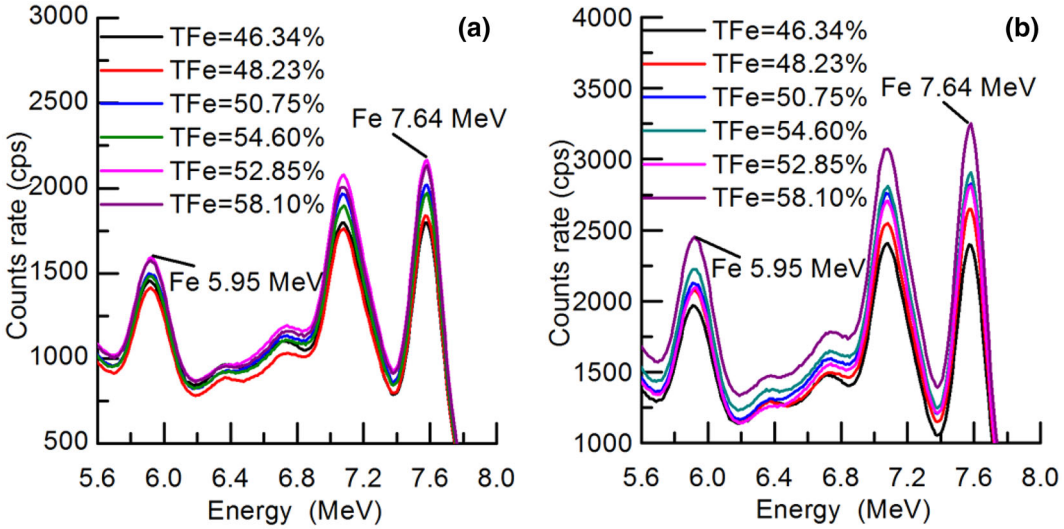

Fig. 4 (Color online) Energy spectra of different samples before (**a**) and after (**b**) gamma-ray self-absorption compensation

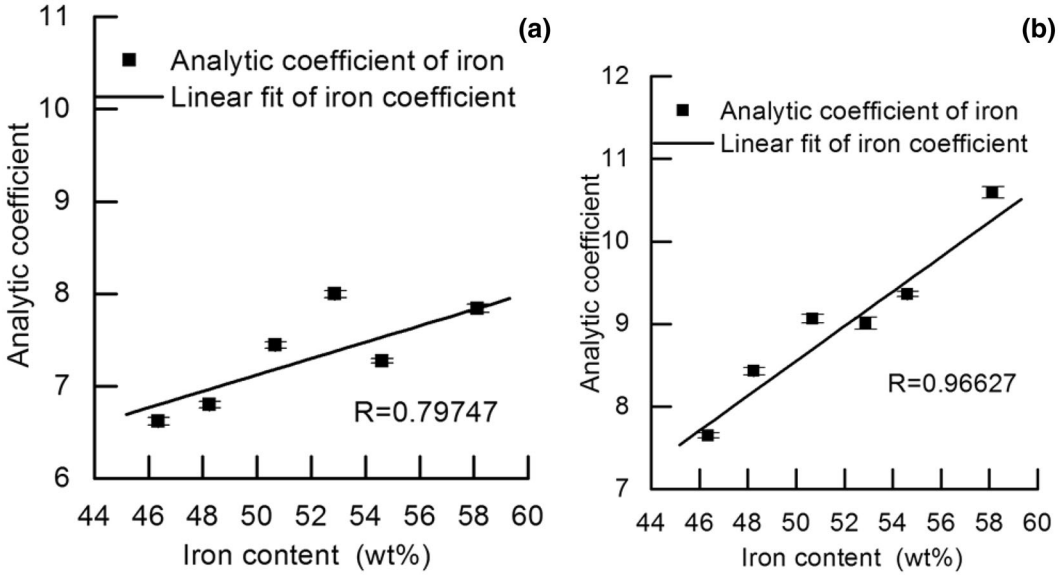

Fig. 5 Relationship between the analytical coefficient and iron content before (**a**) and after (**b**) gamma-ray self-absorption compensation

$$\frac{\partial(m'_{\mathrm{Fe}})}{\partial(N_{\mathrm{element}})} = K\frac{N_{\mathrm{Fe}}\sigma_{\mathrm{Fe}}\sigma^{\mathrm{n}}_{\mathrm{element}}}{(\sum N_i\sigma^{\mathrm{n}}_i)^2} = A\times\sigma^{\mathrm{n}}_{\mathrm{element}} \quad (6)$$

i = Ca, Si, O, Mg, Cl, Fe,

$$A = K\frac{N_{\mathrm{Fe}}\sigma^{\mathrm{n}}_{\mathrm{Fe}}}{(\sum N_i\sigma^{\mathrm{n}}_i)^2} \quad i = \mathrm{Ca, Si, O, Mg, Cl, Fe.} \quad (7)$$

The contribution of iron to the measurement error of the iron grade is:

$$\frac{\partial(m'_{\mathrm{Fe}})}{\partial(N_{\mathrm{Fe}})} = K\frac{(\sum N_i\sigma^{\mathrm{n}}_i - N_{\mathrm{Fe}}\sigma^{\mathrm{n}}_{\mathrm{Fe}})\sigma^{\mathrm{n}}_{\mathrm{Fe}}}{(\sum N_i\sigma^{\mathrm{n}}_i)^2} = A\times\left(\frac{\sum N_i\sigma^{\mathrm{n}}_i - N_{\mathrm{Fe}}\sigma^{\mathrm{n}}_{\mathrm{Fe}}}{N_{\mathrm{Fe}}}\right) \quad (8)$$

i = Ca, Si, O, Mg, Cl, Fe.

The formula for the total error in iron grade detection is:

$$\Delta m'_{\mathrm{Fe}} = A\times\sqrt{0.1856(\Delta N_{\mathrm{Ca}})^2 + 0.0296(\Delta N_{\mathrm{Si}})^2 + 0.0044(\Delta N_{\mathrm{Mg}})^2 + 0.1166(\Delta N_{\mathrm{Fe}})^2 + 1095.61(\Delta N_{\mathrm{Cl}})^2}. \quad (9)$$

Table 7 Neutron capture reaction cross section of element

Element	B	O	Ca	Si	Mg	Fe	Cl
Neutron-absorption cross section (barns)	764	0.00019	0.431	0.172	0.0666	2.56	33.1

Table 8 Comparison data of two experiments

Experiment	Main element	Content (%)	Sample weight (kg)	TNCCSME (mol·barns)
Boron solution	B	0.3	29	6.148
Iron ore concentrate	Fe	56.33	110	2.841

TNCCSME total neutron capture cross section of main element

Formula 9 shows that the changes in the content of chlorine will cause the greatest error in the result. Because chlorine has a large neutron-absorption cross section, the neutron field of the entire system will change considerably when the content of chlorine changes, and, furthermore, it induces more error in the detection of other elements.

The concentration of iron, m_{Fe}, and chlorine, m_{Cl}, can be expressed as follows [20]:

$$m_{\mathrm{Fe}} = (\Phi_0 - \Phi_1)\frac{N_{\mathrm{Fe}}\sigma^{\mathrm{n}}_{\mathrm{Fe}}}{\sum N_i\sigma^{\mathrm{n}}_i} f\eta k_{\mathrm{Fe}} = A^0_{\mathrm{Fe}} k_{\mathrm{Fe}} \quad i = \mathrm{Ca, Si, O, Mg, Cl, Fe}, \tag{10}$$

$$m_{\mathrm{Cl}} = (\Phi_0 - \Phi_1)\frac{N_{\mathrm{Cl}}\sigma^{\mathrm{n}}_{\mathrm{Cl}}}{\sum N_i\sigma^{\mathrm{n}}_i} f\eta k_{\mathrm{Cl}} = A^0_{\mathrm{Cl}} \times k_{\mathrm{Cl}} \quad i = \mathrm{Ca, Si, O, Mg, Cl, Fe}, \tag{11}$$

where Φ_0 and Φ_1 are the neutron flux upon it entering (0) and leaving (1) the sample, A^0_{Fe} is the analytical coefficient of the energy spectrum of iron when the iron content is m_{Fe}, A^0_{Cl} is the analytical coefficient of the energy spectrum of chlorine when the content is m_{Cl}, k_{Fe} and k_{Cl} are scaling factors between the concentration and analytic coefficient, f is the geometric factor for the NaI scintillation detector, and η is the detection efficiency.

When the measured sample changes, the iron and chlorine contents become multiples of the original content p and k, respectively. The corresponding formulas are

$$\begin{aligned} m'_{\mathrm{Fe}} &= pm_{\mathrm{Fe}} \\ &= (\Phi_0 - \Phi'_1)\frac{pN_{\mathrm{Fe}}\sigma^{\mathrm{n}}_{\mathrm{Fe}}}{pN_{\mathrm{Fe}}\sigma^{\mathrm{n}}_{\mathrm{Fe}} + kN_{\mathrm{Cl}}\sigma^{\mathrm{n}}_{\mathrm{Cl}} + N_{\mathrm{O}}\sigma^{\mathrm{n}}_{\mathrm{O}} + N_{\mathrm{Si}}\sigma^{\mathrm{n}}_{\mathrm{Si}} + N_{\mathrm{Ca}}\sigma^{\mathrm{n}}_{\mathrm{Ca}} + N_{\mathrm{Mg}}\sigma^{\mathrm{n}}_{\mathrm{Mg}}} f\eta k'_{\mathrm{Fe}} \\ &= A^1_{\mathrm{Fe}} k'_{\mathrm{Fe}} \end{aligned} \tag{12}$$

$$\begin{aligned} m'_{\mathrm{Cl}} &= km_{\mathrm{Cl}} \\ &= (\Phi_0 - \Phi'_1)\frac{pN_{\mathrm{Cl}}\sigma^{\mathrm{n}}_{\mathrm{Cl}}}{pN_{\mathrm{Fe}}\sigma^{\mathrm{n}}_{\mathrm{Fe}} + kN_{\mathrm{Cl}}\sigma^{\mathrm{n}}_{\mathrm{Cl}} + N_{\mathrm{O}}\sigma^{\mathrm{n}}_{\mathrm{O}} + N_{\mathrm{Si}}\sigma^{\mathrm{n}}_{\mathrm{Si}} + N_{\mathrm{Ca}}\sigma^{\mathrm{n}}_{\mathrm{Ca}} + N_{\mathrm{Mg}}\sigma^{\mathrm{n}}_{\mathrm{Mg}}} f\eta k'_{\mathrm{Cl}} \\ &= A^1_{\mathrm{Cl}} k'_{\mathrm{Cl}} \end{aligned} \tag{13}$$

where Φ'_1 represents the corresponding neutron flux exiting from the surface of the sample, and when the iron content of the sample becomes pm_{Fe}, the chlorine content of the sample becomes km_{Cl}. A^1_{Fe} is the analytical coefficient of the energy spectrum of iron when the iron content is pm_{Fe}, A^1_{Cl} is the analytical coefficient of the energy spectrum of chlorine when the chlorine content is km_{Cl}, and k'_{Fe} and k'_{Cl} are scaling factors.

From Eqs. (10)–(13), the expressions of p and k can be rewritten as:

$$p = \frac{\left(N_{\mathrm{O}}\sigma^{\mathrm{n}}_{\mathrm{O}} + N_{\mathrm{Si}}\sigma^{\mathrm{n}}_{\mathrm{Si}} + N_{\mathrm{Ca}}\sigma^{\mathrm{n}}_{\mathrm{Ca}} + N_{\mathrm{Mg}}\sigma^{\mathrm{n}}_{\mathrm{Mg}}\right)}{\frac{(\Phi_0 - \Phi'_1)}{(\Phi_0 - \Phi_1)} \times \frac{A^0_{\mathrm{Fe}}}{A^1_{\mathrm{Fe}}}\left(\sum N_i\sigma^{\mathrm{n}}_i\right) - \left(\frac{A^0_{\mathrm{Fe}}A^1_{\mathrm{Cl}}}{A^1_{\mathrm{Fe}}A^0_{\mathrm{Cl}}}N_{\mathrm{Cl}}\sigma^{\mathrm{n}}_{\mathrm{Cl}} + N_{\mathrm{Fe}}\sigma^{\mathrm{n}}_{\mathrm{Fe}}\right)} \quad i = \mathrm{Ca, Si, O, Mg, Cl, Fe}, \tag{14}$$

$$k = \frac{\left(N_{\mathrm{O}}\sigma^{\mathrm{n}}_{\mathrm{O}} + N_{\mathrm{Si}}\sigma^{\mathrm{n}}_{\mathrm{Si}} + N_{\mathrm{Ca}}\sigma^{\mathrm{n}}_{\mathrm{Ca}} + N_{\mathrm{Mg}}\sigma^{\mathrm{n}}_{\mathrm{Mg}}\right)}{\frac{(\Phi_0 - \Phi'_1)}{(\Phi_0 - \Phi_1)} \times \frac{A^0_{\mathrm{Cl}}}{A^1_{\mathrm{Cl}}}\left(\sum N_i\sigma^{\mathrm{n}}_i\right) - \left(\frac{A^0_{\mathrm{Cl}}A^1_{\mathrm{Fe}}}{A^1_{\mathrm{Cl}}A^0_{\mathrm{Fe}}}N_{\mathrm{Fe}}\sigma^{\mathrm{n}}_{\mathrm{Fe}} + N_{\mathrm{Cl}}\sigma^{\mathrm{n}}_{\mathrm{Cl}}\right)}. \tag{15}$$

The linear correction factor $g(p, k)$ is defined as:

$$g(p,k) = \frac{(\Phi_0 - \Phi_1)}{(\Phi_0 - \Phi'_1)} \times \frac{pN_{\mathrm{Fe}}\sigma^{\mathrm{n}}_{\mathrm{Fe}} + kN_{\mathrm{Cl}}\sigma^{\mathrm{n}}_{\mathrm{Cl}} + N_{\mathrm{O}}\sigma^{\mathrm{n}}_{\mathrm{O}} + N_{\mathrm{Si}}\sigma^{\mathrm{n}}_{\mathrm{Si}} + N_{\mathrm{Ca}}\sigma^{\mathrm{n}}_{\mathrm{Ca}} + N_{\mathrm{Mg}}\sigma^{\mathrm{n}}_{\mathrm{Mg}}}{N_{\mathrm{Fe}}\sigma^{\mathrm{n}}_{\mathrm{Fe}} + N_{\mathrm{Cl}}\sigma^{\mathrm{n}}_{\mathrm{Cl}} + N_{\mathrm{O}}\sigma^{\mathrm{n}}_{\mathrm{O}} + N_{\mathrm{Si}}\sigma^{\mathrm{n}}_{\mathrm{Si}} + N_{\mathrm{Ca}}\sigma^{\mathrm{n}}_{\mathrm{Ca}} + N_{\mathrm{Mg}}\sigma^{\mathrm{n}}_{\mathrm{Mg}}}. \tag{16}$$

To determine ϕ_0, ϕ_1, and ϕ'_1, a ^{3}He neutron detector was added over the material to detect the neutron flux as shown in Fig. 2. Because the measured material itself slows fast neutrons, ϕ_0 is not the thermal neutron flux when the belt is empty. In this experiment, ϕ_0, the thermal neutron flux, was defined when 20-kg carbon powder was placed on the belt.

The final analytical coefficient is $A^{\mathrm{Final}}_{\mathrm{Fe}} = A^1_{\mathrm{Fe}} \times g(p,k)$. The data used in the calculation of the calibration samples are listed in Table 9. The calibration data are listed in Table 10. The final total iron calibration curve is shown in Fig. 6.

Table 9 Neutron self-absorption correction parameters and data of the six calibration samples

Sample	1-1#	1-2#	1-3#	1-4#	1-5#	1-6#
A_{Fe}^{0}	9.063	9.063	9.063	9.063	9.063	9.063
A_{Cl}^{0}	0.018	0.018	0.018	0.018	0.018	0.018
A_{Fe}^{1}	7.648	8.428	9.063	9.36	9.008	10.594
A_{Cl}^{1}	0.048	0.038	0.018	0.008	0.026	0.001
p	0.921	0.958	1	1.084	1.044	1.147
k	2.91	2.175	1	0.467	1.517	0.054
$\phi_0 - \phi_1$	644.2	644.2	644.2	644.2	644.2	644.2
$\phi_0 - \phi_1'$	653.2	670	644.2	629.3	666.7	684.9
$g(p, k)$	1.091	1.03	1	1.05	1.05	0.981
A_{Fe}^{Final}	8.347	8.684	9.063	9.826	9.459	10.393

2.5 Calculation of check samples

To verify the reliability of the method, nine validation samples were prepared. The experimental data of each sample are listed in Table 11. The total iron content comparison curve of the validation samples is shown in Fig. 7.

3 Results and discussion

The experiment adopts the spectrum library least-squares approach to analyze the spectrum, effectively eliminating the influence of interference elements. The spectrum library was established before the experiment and contains the characteristic energy spectra of calcium, silicon, iron, aluminum, magnesium, chlorine, sulfur, sodium, and the background. Through the least-squares operation, the contribution of each element in the total spectrum can be found, which corresponds to the content of the element.

Because of the strong gamma-ray self-absorption and neutron-absorption effect of iron, the PGNAA detection result is quite poor, and thus, both gamma-ray self-absorption correction and neutron self-absorption correction should be incorporated into PGNAA detection.

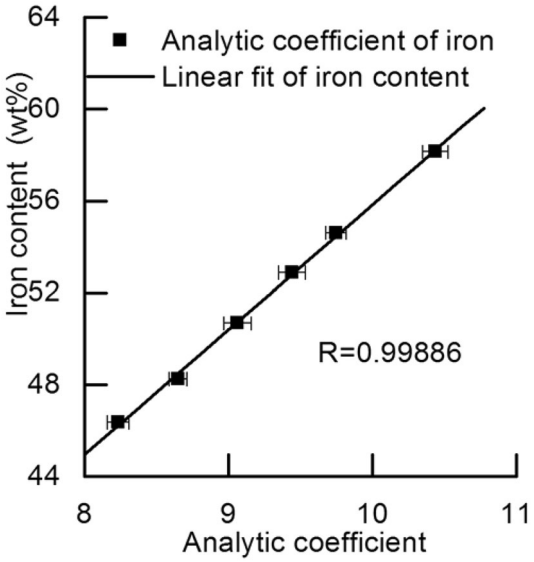

Fig. 6 Iron calibration curve

Figure 4b shows the compensation effect of energy spectra at different iron concentrations. Figure 5a, b gives the relationship between the analytical coefficient and the iron content before and after gamma-ray self-absorption correction, respectively. Before compensation, the linear correlation coefficient between the analytical coefficient and the iron content is 0.79747 and is improved to 0.96627 after energy spectrum compensation.

Owing to the large neutron capture cross section of iron and chlorine, which considerably disturbs the iron grade detection result, the experimental results should be corrected to eliminate the interference of chlorine. As shown in Fig. 6, after neutron self-absorption correction and chlorine interference correction, the linear correlation coefficient between iron content and the analytical coefficient reaches 0.99886.

Figure 7 shows the total iron content comparison curve of the validation samples, in which the trend of calculated value is consistent with the actual value. The RMS error of the validation samples is 0.45, which is the ideal result.

Table 10 Calibration data of the six calibration samples

Sample	1-1#	1-2#	1-3#	1-4#	1-5#	1-6#
Calculate iron content (wt%)	46.41	48.33	50.49	54.83	52.74	58.06
Laboratory iron content (wt%)	46.34	48.23	50.75	54.6	52.85	58.1
Absolute error (wt%)	0.07	0.1	− 0.26	0.23	− 0.11	− 0.04
RMS error (wt%)	0.16					

RMS root mean square

Table 11 Calculation parameters and data of nine check samples

Samples	2-1#	2-2#	2-3#	2-4#	2-5#	2-6#	2-7#	2-8#	2-9#
A_{Fe}	6.674	7.054	7.501	7.296	6.977	7.756	7.852	7.698	7.624
N/N_0	0.532	0.503	0.556	0.487	0.558	0.591	0.529	0.533	0.451
A_{Fe}^0	9.063	9.063	9.063	9.063	9.063	9.063	9.063	9.063	9.063
A_{Cl}^0	0.018	0.018	0.018	0.018	0.018	0.018	0.018	0.018	0.018
A_{Fe}^1	8.001	8.72	8.702	9.23	8.316	9.051	9.792	9.175	9.942
A_{Cl}^1	0.044	0.028	0.033	0.014	0.031	0.022	0.013	0.018	0.005
p	0.925	0.99	1.001	1.045	0.942	1.017	1.08	1.059	1.111
k	2.556	1.601	1.912	0.798	1.761	1.245	0.722	1.046	0.281
$\phi_0 - \phi_1$	644.2	644.2	644.2	644.2	644.2	644.2	644.2	644.2	644.2
$\phi_0 - \phi_1'$	662.3	639.6	644.2	655.1	670.2	656.3	641.1	650.5	673.5
$g(p, k)$	1.046	1.029	1.043	1.027	1.023	1.019	1	1.046	1.012
A_{Fe}	8.39	8.972	9.074	9.475	8.566	9.219	9.789	9.6	10.066
Calculate iron content (wt%)	47.21	50.32	50.86	53.01	48.15	51.64	54.69	53.67	56.16
Laboratory iron content (wt%)	47.29	49.49	50.54	52.68	48.55	51.8	55.48	53.73	56.35
Absolute error (wt%)	− 0.08	0.83	0.32	0.33	− 0.4	− 0.16	− 0.79	− 0.06	− 0.19
RMS error (wt%)	0.45								

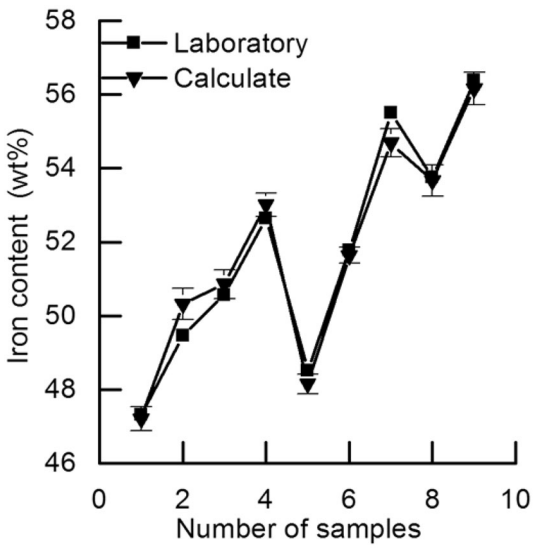

Fig. 7 Check samples comparison curve

4 Conclusion

Based on the PGNAA technique and a new correction algorithm, the linear correlation coefficient between the total iron content and analytical coefficient of six calibration samples was improved to 0.99886, and the RMS error of nine validation samples was decreased to 0.45, which is the ideal result. The PGNAA technique can be applied to real-time heavy element concentrate detection.

References

1. F.Y. Shi, J.Y. Ma, J.W. Zhao et al., Detection sensitivities of C and O in coal due to a channel in the moderator. Radiat. Meas. **46**, 88–91 (2011). https://doi.org/10.1016/j.radmeas.2010.08.025
2. A.A. Naqvi, A Monte Carlo comparison of PGNAA system performance using ^{252}Cf neutrons, 2.8-MeV neutrons and 14-MeV neutrons. Nucl. Instrum. Methods A **511**, 400–407 (2003). https://doi.org/10.1016/s0168-9002(03)01949-1
3. A. Favalli, H.C. Mehner, V. Ciriello et al., Investigation of PGNAA using the LaBr 3 scintillation detector. Appl. Radiat. Isot. **68**, 901–904 (2010). https://doi.org/10.1016/j.apradiso.2009.09.058
4. C. Oliveira, J. Salgado, F. Leitao, Density and water content corrections in the gamma count rate of a PGNAA system for cement raw material analysis using the MCNP Code. Appl. Radiat. Isot. **49**, 923–930 (1998). https://doi.org/10.1016/s0969-8043(97)10111-7
5. A.X. da Silva, V.R. Crispim, Moderator-collimator-shielding design for neutron radiography systems using ^{252}Cf. Appl. Radiat. Isot. **54**, 217–225 (2001). https://doi.org/10.1016/s0969-8043(00)00291-8
6. C. Oliveira, J. Salgado, I.F. Goncalves et al., A Monte Carlo study of the influence of the geometry arrangements and structural materials on a PGNAA system performance for cement raw material analysis. Appl. Radiat. Isot. **48**, 1349–1354 (1997). https://doi.org/10.1016/s0969-8043(97)00130-9
7. J.B. Yang, X.G. Tuo, Z. Li et al., Mc simulation of a PGNAA system for on-line cement analysis. Nucl. Sci. Tech. **21**, 221–226 (2010). https://doi.org/10.13538/j.1001-8042/nst.21.221-226
8. A.A. Naqvi, M.M. Nagadi, Performance comparison of an ^{241}Am-Be neutron source-based PGNAA setup with the KFUPM PGNAA setup. J. Radioanal. Nucl. Chem. **260**, 641–646 (2004). https://doi.org/10.1023/b:jrnc.0000028225.07280.74
9. F. Zhang, J.T. Liu, Monte Carlo simulation of PGNAAsystem for determining element content in the rock sample. J. Radioanal.

Nucl. Chem. **299**, 1219–1224 (2014). https://doi.org/10.1007/s10967-013-2858-3
10. L.Z. Zhang, B.F. Ni, W.Z. Tian et al., Status and development of prompt γ-ray neutron activation analysis. Atom. Energy Sci. Technol. **39**, 282–288 (2005). https://doi.org/10.3969/j.issn.1000-6931.2005.03.022. **(in Chinese)**
11. W. Zhang, L. Zhao, Y.F. Li, Neutron activation analyzer radiological monitoring system. Mod. Min. **8**, 188–189 (2017). https://doi.org/10.3969/j.issn.1674-6082.2017.08.059
12. C.S. Lim, J.R. Tickner, B.D. Sowerby et al., An on-belt elemental analyser for the cement industry. Appl. Radiat. Isot. **54**, 11–19 (2001). https://doi.org/10.1016/S0969-8043(00)00180-9
13. Q.F. Song, Y.L. Gong, W. Zhang et al., Feasibility study for on-line analysis of bauxite using a PGNAA system. China Min. Mag. **10**, 171–174 (2015). https://doi.org/10.3969/j.issn.1004-4051.2015.10.037. **(in Chinese)**
14. B.R. Wang, G.H. Yin, Z.P. Yang, Identification system for chemical warfare agents with PGNAA method. Nucl. Electron. Detect. Technol. **27**, 621–623 (2007). https://doi.org/10.3969/j.issn.0258-0934.2007.04.002. **(in Chinese)**
15. Y.L. Gong, W. Zhang, J.T. Tao, et al. CN 201348615Y, Adjustable multi element analyzer, 2008
16. C. Cheng, W.B. Jia, D.Q. Hei et al., Study of influence of neutron field and γ-ray self-absorption on PGNAA measurement. Atom. Energy Sci. Technol. **48**, 802–806 (2014). https://doi.org/10.7538/yzk.2014.48.s0.0802. **(in Chinese)**
17. M.E. Medhat, Gamma-ray attenuation coefficients of some building materials available in Egypt. Ann. Nucl. Energy **36**, 849–852 (2009). https://doi.org/10.1016/j.anucene.2009.02.006
18. L.T. Yang, C.F. Chen, X.X. Jin et al., Research on accurate calculation method of γ-ray self-absorption correction factor. Atom. Energy Sci. Technol. **51**, 323–329 (2017). https://doi.org/10.7538/yzk.2017.51.02.0323. **(in Chinese)**
19. Reedy and Frankle, At. Data Nucl. Data Tables 80, 1, 2002. https://www-nds.iaea.org/pgaa. Accessed 9 Mar 2019
20. W.B. Jia, C. Cheng, Q. Shan et al., Study on the elements detection and its correction in aqueous solution. Nucl. Instrum. Methods B **342**, 240–243 (2015). https://doi.org/10.1016/j.nimb.2014.10.010
21. K. Sudarshan, R. Tripathi et al., A simple method for correcting the neutron self-shielding effect of matrix and improving the analytical response in prompt gamma-ray neutron activation analysis. Anal. Chim. Acta **549**, 205–211 (2005). https://doi.org/10.1016/j.aca.2005.06.021
22. Z.H. Wu, H.Q. Qi, N.X. Shen et al., *Experimental Method of Nuclear Physics* (Atomic Energy Press, Beijing, 1997), pp. 65–66. **(in Chinese)**